

OECD MCCI Project
Small-Scale Water Ingression and Crust Strength Tests (SSWICS)
Final Report: Category 1 Test Results

Rev. 1 - Final

November 2010

by:

S. Lomperski, M. T. Farmer, R. W. Aeschlimann, and D. J. Kilsdonk

Nuclear Engineering Division
Argonne National Laboratory
9700 S. Cass Avenue
Argonne, IL 60439 USA

Table of Contents

EXECUTIVE SUMMARY ii

1.0 INTRODUCTION..... 1

2.0 SPARGING TESTS 2

 2.1 Gas Sparging System Description..... 2

 2.2 Sparging System Limitations 4

 2.3 Test Apparatus Overview..... 6

 2.4 Instrumentation 9

 2.5 Results 11

3.0 CRUST STRENGTH TESTS 16

 3.1 Test Results 16

4.0 REFERENCES..... 21

List of Figures

Figure	Page
2-1 SSWICS-8 Stainless Steel Capillary Layout; Capillary Tips Flush with Basemat Surface (dimensions in mm)	3
2-2 SSWICS-11 Tungsten Tube Layout (array pitch identical to that of SSWICS-8). Capillaries Extend 50 mm Above the Basemat.....	3
2-3 Sparging System Side View	5
2-4 Photo of SSWICS-11 Basemat with Tungsten Capillaries	5
2-5 Melt Temperature Dependence of Superficial Velocity and Power Absorbed by Injected Argon	6
2-6 Side View of SSWICS-11 Reaction Vessel.....	7
2-7 SSWICS Melt Quench Facilit.....	8
2-8 Instrumentation Positions in Basemat and Lower MgO Liner	9
2-9 Corium Side View of Ingot 11.....	12
2-10 Corium at Level of Top of Tungsten Thermowell after Removal of Upper Layers (Ingot 11).....	12
2-11 Top View of Ingot-6 Ingot Within Liner	13
2-12 Top View of Ingot-11 Ingot before Liner Removal	13
2-13 SSWICS-11 Temperatures in Tungsten Thermowell	14
2-14 SSWICS-11 Calculated Corium Surface Heat Flux	14
2-15 Heat Flux for Tests with Sparging (11) and Without (8 & 6). The Melt Composition and Quench Conditions are Identical for the Three Tests.....	15
2-16 Calculated Heat Flux for all Nine Quench Tests	15
3-1 Side View of Reaction Vessel for SSWICS-9 and -10	17
3-2 Ingot 10 Load Test.....	20
3-3 Measured Strength of SSWICS Room Temperature Samples and In-Situ Measurements of Crust Strength in CCI-1 and CCI-3.....	20

List of Tables

Table	Page
2-1 Instrument List.....	10
3-1 Test Specifications for SSWICS Quench Experiments	18
3-2 Source Data for Calculation of Section Strength.....	19

EXECUTIVE SUMMARY

A series of separate-effects experiments was conducted under the MCCI-1 program to investigate the influence of melt composition on quench rate and crust strength. Seven quench tests using 75 kg melts demonstrated that melt cooling is enhanced by water ingression made possible via thermal stress-induced cracking, and that the role of water ingression increases as concrete content decreases. The tests employed flooding from above, an inert basemat (MgO rather than concrete), and excluded sparging gases. Load tests performed on sectioned ingots, the byproduct of the quench tests, indicated that the material is rather weak and suggested that a corium crust is unlikely to have the strength to be self-supporting in a plant-scale, anchored crust configuration. The test series left one issue open and raised a second: 1) how would the sparging gases expected from the decomposition of concrete affect the dryout heat flux, and 2) did sectioning the ingots weaken them and lead to an unduly low assessment of crust strength? These two issues were addressed by four tests conducted in the MCCI-2 program and are the subject of this report.

Sparging gases were simulated in two tests, denoted SSWICS-8 and -11, by injecting argon through capillaries embedded within the basemat. Gases generated at the bottom of the melt are propelled up through the corium by buoyancy forces and this has the potential to create melt porosity, which may supplement the fissures induced by thermal stress cracking and enhance water ingression cooling. The composition of both melts was 56% UO₂, 23% ZrO₂, 7% Cr, and 14% siliceous concrete, identical to that of SSWICS-6 in the first quench series. For SSWICS-8, the ends of the capillaries were flush with the surface of the basemat, i.e., at the level of the corium/MgO interface at the bottom of the melt. The test data indicated that the sparging gases travelled around the melt rather than through it, and so the test was effectively a repeat of SSWICS-6 and could not provide an indication of the effects of sparging gases. It did, however, serve to demonstrate test repeatability as the cooling rates of SSWICS-6 and -8 are well matched. SSWICS-11 is a repeat of SSWICS-8 with capillaries extended 50 mm above the basemat to discourage gases from circumventing the melt. The modification proved successful and SSWICS-11 cooled considerably faster than either SSWICS-8 or -6. Moreover, the morphology of the ingot was unusual, exhibiting a porous structure lacking in any of the previous ingots. The test indicated that the sparging gases can indeed markedly influence both the morphology and cooling rate of the corium.

SSWICS-9 and -10 were commissioned to address the possibility that cutting ingots into thinner sections contributes to the existing crack structure and weakens samples before load testing. Ingots produced by the first seven tests were sectioned because, at a height of 15 cm, they were too thick to fail in the desired mode when loaded with the apparatus designed to measure sample strength. This uncertainty is eliminated for the new tests by reducing the corium charge to 25 kg so that the quench process will produce a 5 cm high ingot that can be load tested without first experiencing the sectioning process. Both SSWICS-9 and -10 quench tests successfully created the desired ingots, but only Ingot-10 was sturdy enough to survive removal from the quench test apparatus and placement into the loading apparatus. Ingot-9 broke apart upon removal from the basemat. The chemical composition of Ingot-10 was 61% UO₂, 25% ZrO₂, 6% Cr, and 8% siliceous concrete, identical to that of Ingot-2 in the first quench series. The measured strength of Ingots-2 and -10 are 1.1 ±0.2 MPa and 1.0 ±0.3 MPa, respectively, effectively identical given the level of measurement uncertainty. Though we have only a single measurement of the strength of an uncut crust sample, it supports the notion that the cutting process does not unduly weaken the samples. Moreover, it is noted that Ingot-9 proved too fragile for loading in part because it did not bond to the MgO liner. All the samples suitable for loading, both cut and uncut, were supported in part by this outer ring of MgO. This suggests that the MgO contributes to the effective strength of the ingots and that the measurements are conservative.

Below is a summary table of the conditions for the SSWICS-1 through -11:

Test Specifications for SSWICS Quench Experiments

Parameter	Test Number										
	1	2	3	4	5	6	7	8	9	10	11
Melt composition (wt% UO ₂ /ZrO ₂ /Cr/Concrete)	61/25/6/8	61/25/6/8	61/25/6/8	48/20/9/23	56/23/7/14	56/23/6/14	64/26/6/4	56/23/6/14	56/23/6/14	61/25/6/8	56/23/6/14
Concrete type	LCS	SIL	LCS	LCS	LCS	SIL	LCS	SIL	SIL	SIL	SIL
Melt mass (kg)	75	75	75	60	68	68	80	68	23	25	68
Melt depth (cm)	15	15	15	15	15	15	15	15	5	5	15
Initial Melt Temperature (°C)	~2300	~2100	~2100	~2100	~2100	~1950	~2100	~1900	-	-	~1850
System pressure (bar)	1	1	4	4	4	1	4	1	1	1	1
Water injection flowrate (lpm)	4	4	12	13	6	14	13	10	9	9	-
Water injected (liters)	33	39	34	40	61	47	40	41	20	29	>30
Test date (day/mo/year)	30/08/02	17/09/02	30/01/03	13/03/03	15/10/03	24/02/04	14/12/04	25/01/07	14/02/08	5/03/08	11/05/08

1.0 INTRODUCTION

Seven small-scale water ingression tests were performed during the first MCCI program (MCCI-1) to evaluate debris cooling mechanisms identified in the Melt Attack and Coolability Experiments (MACE). In particular, the tests were designed to measure the dependence of dryout heat flux on corium composition and system pressure for melts flooded from above. Tests were performed with 75 kg melts made up of UO_2 and varying amounts of either siliceous or limestone common sand concrete. The concrete contents varied from a low of 4 wt% to a high of 23 wt% and the melts were quenched at pressures of either 1 or 4 bar. These tests demonstrated that melt cooling can be enhanced by water ingression made possible by thermal stress-induced cracking, and that the role of water ingression increases as concrete content decreases. The dependence of water ingression cooling rate on concrete content is strongest for melts containing less than 14% concrete. For melts with 14% or more concrete, little evidence of water ingression cooling was discernible. It was also found that melts with siliceous concrete cooled at about the same rate as melts with a similar amount of limestone common sand concrete.

A second element of the MCCI-1 program involved evaluating the strength of corium crusts produced by the flooding and quench process. Interest in this area arose during the MACE program when the large-scale tests were seen to produce crusts that anchored to the sides of the test section, thermally isolating the overlying water layer from the melt below. Such decoupling is not expected for a typical reactor cavity where the lateral span is much larger, ~5-6 m. Instead, the crust is expected to fracture under the weight of the coolant and the crust itself so that coolant contact with the melt is maintained. However, because of a lack of knowledge of the strength of the crust, one cannot be certain that it would actually fracture under such circumstances. This issue was addressed with an apparatus designed to mechanically load the corium samples produced by the quench tests, which are formed as $\phi 30 \times 15$ cm ingots. It could be seen that a network of cracks ran through each ingot, presumably the result of thermal stress-induced cracking. Ingots were sliced into 5-10 cm-thick slabs to increase the aspect ratio and improve the measurement of crust fracture strength. The slabs were tested individually by placing them upon a thin annular support ring and loaded with a piston until they fractured. The strength of these samples was found to be far below that of unflawed concrete or UO_2 . The data suggests that corium crusts are not strong enough to be self-supporting at plant scale.

The quench tests carried out for MCCI-1 utilized an inert basemat, thus excluding the sparging gases that are expected from the decomposition of concrete during an actual MCCI. It is thought that these gases may influence the morphology of the crust along with its strength and, indirectly, the melt cooling rate. The separate effects tests of MCCI-1 were not designed to address this issue. A second open issue is associated with the act of cutting the ingots before they were tested for strength. Since cracks permeated each ingot prior to sectioning, it was not clear whether the process added additional cracks and further weakened the samples. Four tests in the MCCI-2 program were assigned to address these two issues, which can be summarized as:

- 1) How would sparging gases affect the cooling rate and morphology of the melt compared to that of the previous melts quenched with an inert basemat?
- 2) Did sectioning the ingots weaken them and lead to an unduly low assessment of crust strength?

This report describes the results of SSWICS-8 through -11 (small scale water ingression and crust strength) performed as part of the OECD-sponsored MCCI-2 program. Two tests were devoted to the sparging issue and two to uncertainty in measured crust strength. Though there is no direct connection between these two issues, they are both included under the program heading of “category 1” tests and so

they are treated together here. The report begins with the results of sparging tests SSWICS-8 and -11 and then covers the effort to assess the influence of cutting corium ingots through SSWICS-9 and -10.

2.0 SPARGING TESTS

One aim of MCCI-2 is to investigate the role of gas sparging on the corium cooling rate. The gases are a byproduct of the decomposition of concrete, which occurs when the material overheats. Gases generated near the corium/concrete interaction zone at the bottom of the melt are propelled up through the corium by buoyancy forces and the resultant gas flow has the potential to create melt porosity. This porosity is expected to supplement the fissures induced by thermal stress cracking. These extra pathways could enhance the amount of water ingress cooling and quench the melt more rapidly than cases lacking sparging gases. Alternatively, the upward movement of noncondensable gas could hinder the downward flow of water into cracks with the result being degradation in cooling rate.

All seven quench tests conducted during the previous program utilized an inert MgO basemat and excluded sparging gases to better isolate the effects of melt composition on cooling rate. A table summarizing test parameters can be found in both the executive summary and in Section 3.1. For two tests in the MCCI-2 program, SSWICS-8 and -11, sparging gases were included. The melt composition and quench conditions were matched to those of SSWICS-6 (56% UO₂, 23% ZrO₂, 7% Cr, and 14% siliceous concrete, 1 bar pressure) to allow a direct determination of the influence of gas on morphology and cooling rate. The SSWICS facility is not equipped to heat the melt to simulate fission product decay heat and so replacement of the MgO basemat with a concrete basemat would not be useful in generating a continuing supply of gas from decomposing concrete. Instead, the facility was outfitted with a system to inject gas through a network of capillaries in the basemat, allowing precise control of the injection rate. The system configuration for SSWICS-8 and -11 is described below.

2.1 Gas Sparging System Description

The MACE MSET-1 injector pitch was deemed suitable for the SSWICS injector since the distance is less than the expected bubble diameter [1]. The MSET-1 injector was a plate with 1 mm i.d. holes arranged on a square pitch of 38 mm, which produced a hole density of ~7 holes/100 cm². Figure 2-1 provides a top view of the basemat showing the capillary layout for SSWICS-8. A total of 44 capillaries were used, each having an inner and outer diameter of 0.57 and 1.5 mm, respectively. The capillaries were all linked to a common plenum. The reason for using capillaries in this fashion is that the system can generate low flow rates with relatively high pressure drops. A high pressure drop reduces flow fluctuations associated with changes in the downstream (reaction vessel) pressure, which can vary with, for example, liquid level. An equal flow distribution is achieved by simply matching the capillary lengths.

The tips of the capillaries were made flush with the basemat surface as it was considered pointless to extend them above the basemat and into the melt since the initial thermite temperature is 2000°C and steel melts at 1400°C. After SSWICS-8 was conducted it was found that, unfortunately, the sparging gases moved laterally across the basemat under the melt and escaped without passing through the melt. It is thought that shortly after thermite ignition a thin crust quickly formed between the melt and the basemat, preventing gas flow up through the melt [2]. No gas travelled through the melt during SSWICS-8 and so it was effectively a repeat of SSWICS-6 and unable to provide information on the effects of sparging. The remainder of this section covers SSWICS-11, which was given a modified injection system that successfully prevented gas from bypassing the melt.

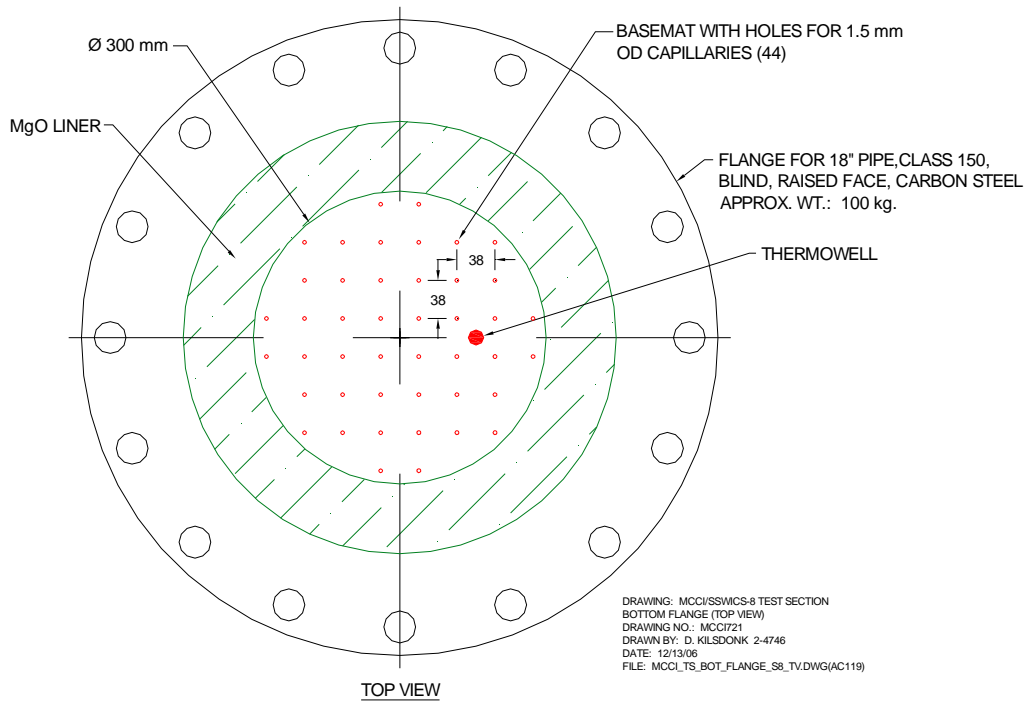


Figure 2-1. SSWICS-8 Stainless Steel Capillary Layout; Capillary Tips Flush with Basemat Surface (dimensions in mm).

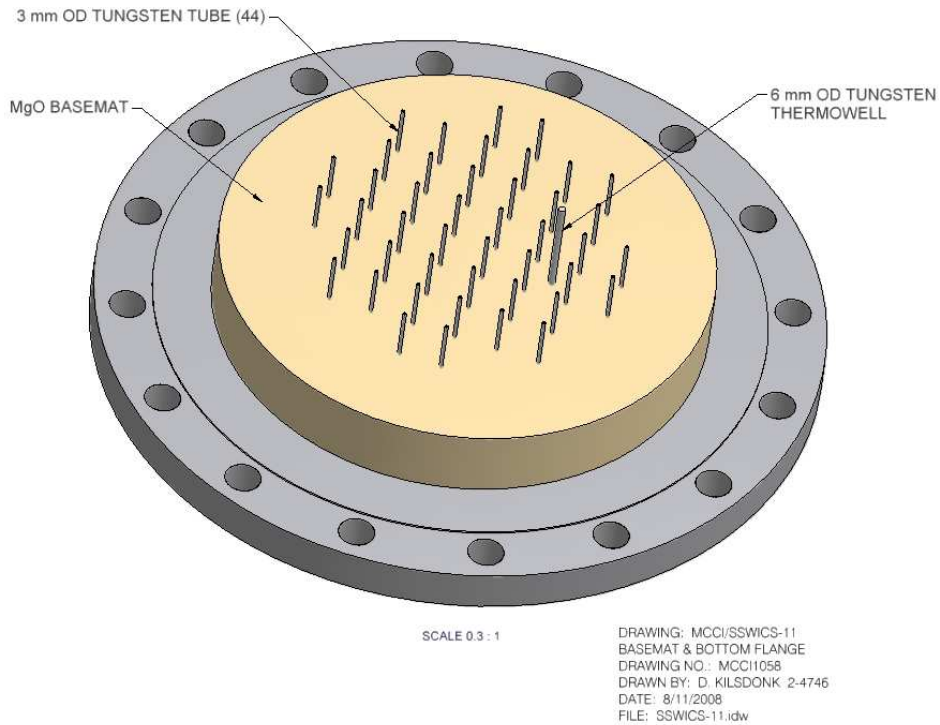


Figure 2-2. SSWICS-11 Tungsten Tube Layout (array pitch identical to that of SSWICS-8). Capillaries Extend 50 mm Above the Basemat.

The new configuration for SSWICS-11 introduced tubes extending 50 mm above the basemat and into melt, which is 150 mm deep. An isometric view of the layout is shown in Figure 2-2. Because the initial temperature of the corium is so high, the tubes must be made of a refractory material. Ceramics are unlikely to withstand the thermal shock of thermite ignition and so tungsten was selected. The tubes have an outer diameter of 3 mm (1/8"), which was the smallest available for tubes of sufficient length to extend down through the basemat, the flange, and the compression fitting. The inner diameter is 1.6 mm.

As in SSWICS-8, the total number of tubes is 44 and the pitch 38 mm. A Swagelok fitting connects each tube to a capillary. Figure 2-3 shows a side view of the reaction vessel and injection system. A photo of the basemat is provided in Figure 2-4.

Within the melt the tubes act as cooling fins drawing heat down into the flange, which increases undesired heat losses. This source of heat loss was estimated to be no more than 800 W near the beginning of the test when the melt temperature is highest, falling as the melt cools. This corresponds to roughly 5% of the initial cooling rate and was deemed acceptable.

2.2 Sparging System Limitations

The sparging system has two particular characteristics that should be noted: 1) it delivers gas at a constant mass flow rate rather than a constant melt superficial velocity, and 2) the gas is not preheated before injection. This section describes how these characteristics influence the gas sparging test.

A key specification for a gas sparging test is the gas injection rate. This parameter is most conveniently defined in terms of a melt superficial gas velocity. The approach has been to specify a particular superficial gas velocity to be established at the very beginning of a test. The flow controller is then set to deliver the rate that produces the desired initial test condition. The flow controller set point is calculated with the assumption that the injected gas will be instantaneously heated to the melt temperature. The initial condition for SSWICS-8 was 2 cm/s at the beginning of the test with a presumed initial melt temperature of 2000°C. The flow controller was set to a constant 11 slpm (standard liters/minute).

The flow controller effectively maintains a constant mass flow rate and so, as the melt cools, the superficial gas velocity drops. Figure 2-5 illustrates the velocity drop that can be expected during the course of the test. At the end, when the melt has cooled to 100°C, the gas velocity has dropped by a factor of six to 0.3 cm/s. Though this is a large change, much of it may be irrelevant with regards to the creation of melt porosity since the corium is in solid form for much of the quench test. Shown in Figure 2-5 is the approximate lower limit melt solidus temperature. Below ~1100°C the melt is completely solid and the gas cannot influence the corium permeability. The plot shows that between the initial temperature of 2000°C and the solidus limit of 1100°C, the superficial velocity drops only 40%. In summary, one should be aware that the sparging system does not maintain a constant superficial gas velocity throughout the test. There is a large drop in velocity, but much of it occurs after the melt has solidified.

Figure 2-5 also shows the heat transfer rate from melt to the injected argon as it is heated from room temperature to the melt temperature. Like conduction losses through the capillaries, this is undesirable heat transfer as the experiment is intended to measure the heat transfer rate from the melt to the overlying water layer. It can be seen that the power is highest (1.6 kW) at the beginning of the test when the melt is at peak temperature, declining to less than 1 kW at the solidus temperature of 1100°C. This can be compared with typical melt cooling rates during past tests: ~10 kW shortly after water has been added to the melt and ~3-4 kW by the time the temperature drops to ~1000°C. Thus the thermal

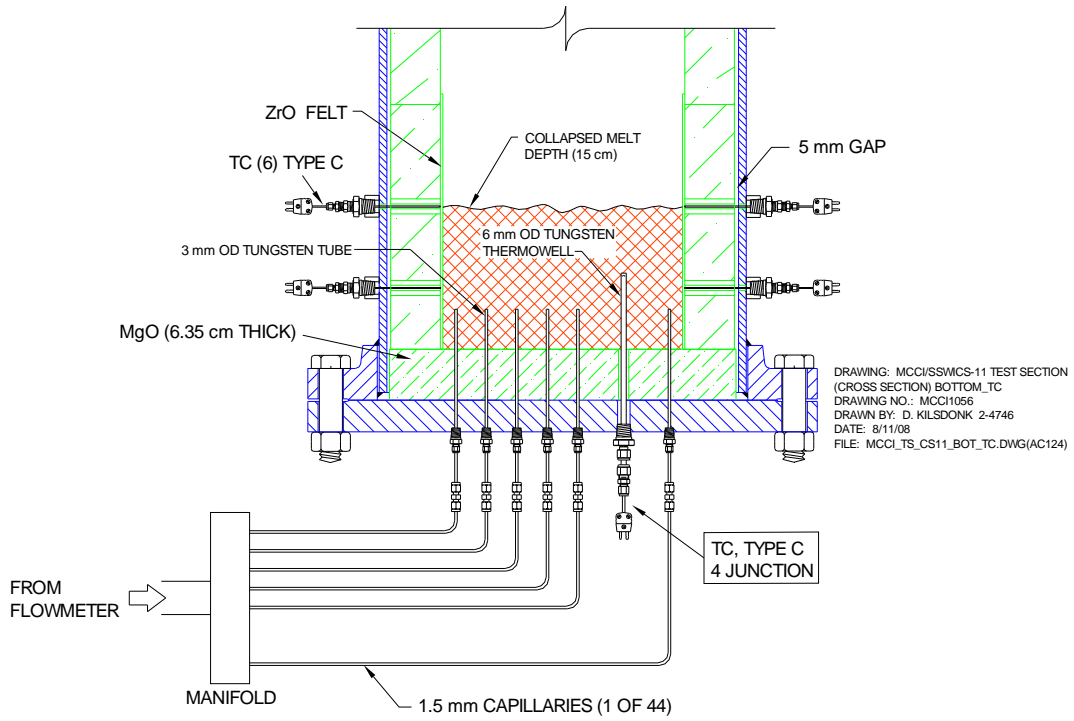


Figure 2-3. Sparging System Side View.



Figure 2-4. Photo of SSWICS-11 Basemat with Tungsten Capillaries.

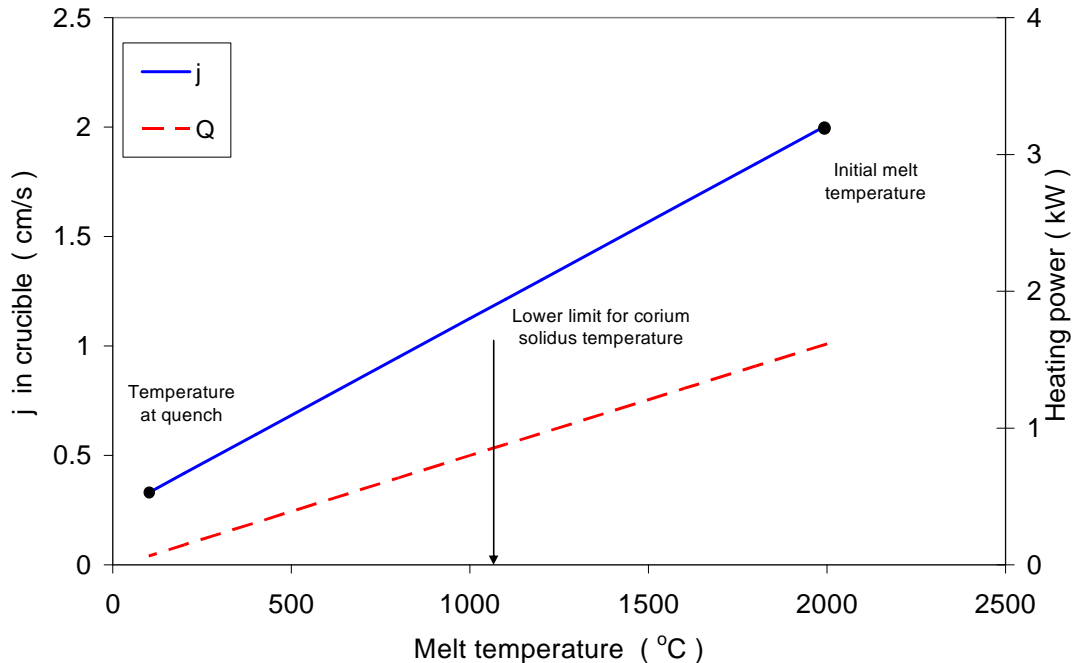


Figure 2-5. Melt Temperature Dependence of Superficial Velocity and Power Absorbed by Injected Argon.

power heating the gas from room temperature to the melt temperature was expected to be equivalent to, very roughly, ~15% of the initial cooling power via surface boiling, increasing to ~25% as the melt reaches the solidus temperature. These loss levels are significant and so gas preheating was considered. It was not implemented due to technical difficulties and limited benefits [3]. The formation of melt porosity by the gas is thought to be unaffected, or only indirectly affected by these additional heat losses.

2.3 Test Apparatus Overview

The SSWICS reaction vessel (RV) has been designed to hold up to 100 kg of melt at an initial temperature of 2500°C. The RV lower plenum consists of a 67.3 cm long, 45.7 cm outer diameter carbon steel pipe (Figure 2-6). The pipe is insulated from the melt by a 6.4 cm thick layer of cast MgO. The selected pipe and insulation dimensions result in a melt diameter of 30.5 cm and a surface area of 730 cm². The melt depth at the maximum charge of 100 kg is about 20 cm.

The RV lower flange is insulated with a 6.4 cm thick slab of cast MgO that spans the entire inner diameter of the pipe. The MgO slab and sidewalls form the crucible containing the corium. This particular geometry was chosen to facilitate removal of the slab for the crust strength measurement tests. Corium has a tendency to bond with the MgO insulation and this design normally allows one to pull the corium ingot off the basemat without damage.

The RV upper plenum consists of a second section of pipe lined with stainless steel. The role of this liner is to protect the walls of the reaction vessel upper plenum from the heat of thermite ignition. Three 10 cm pipes welded near the top of the vessel provide 1) a vent line for the initial surge of hot noncondensable gases generated by the thermite reaction, 2) a pressure relief line with a rupture disk (7.7 bar at 100°C), and 3) an instrument flange for the absolute pressure transmitter that measures the reaction vessel pressure. Four 6 mm tubes serve as water inlets for melt quenching. A baffle is mounted

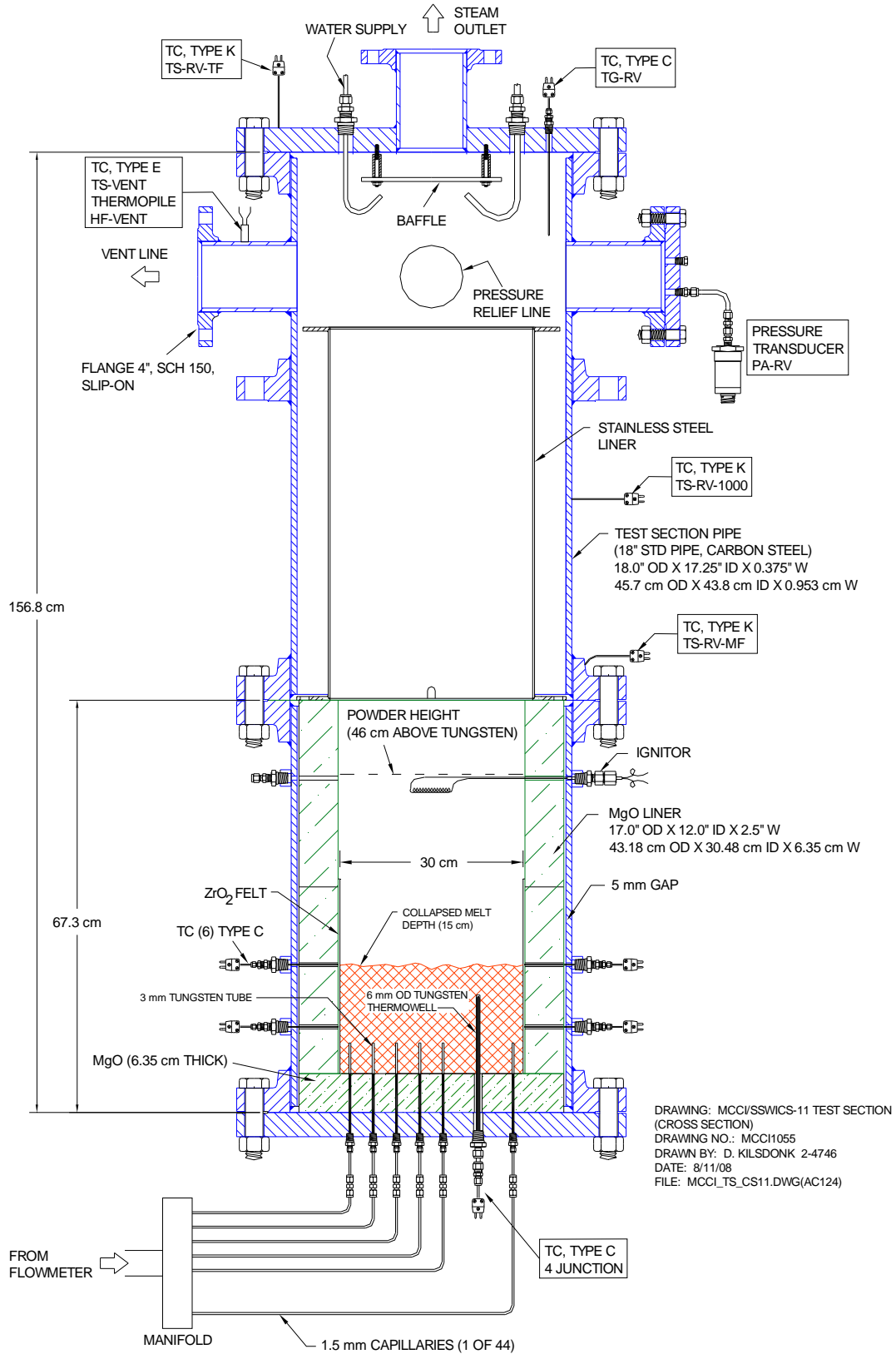


Figure 2-6. Side View of SSWICS-11 Reaction Vessel.

below the upper flange and the water flow is directed towards the baffle to reduce the momentum of the fluid before it drops down onto the melt. The baffle is also intended to prevent water droplets from being carried up towards the condenser, which would adversely affect the heat flux measurement. A fourth 10 cm pipe welded to the top flange provides an outlet to carry steam from the quenching melt to four cooling coils. A control valve on the line allows pressure regulation for tests carried out at elevated pressure. The water-cooled coils are used to condense the steam flowing from the RV, and the condensate is collected within a 200 cm high, 20 cm diameter condensate tank (CT). Figure 2-7 is a schematic that provides an overview of the entire SSWICS melt-quench facility.

2.4 Instrumentation

Instrumentation was selected to provide the measurements necessary to determine the melt dryout heat flux. The critical measurement for these tests is the steaming rate in the RV, which is found indirectly by measuring the rate of condensate collection in the CT. A differential pressure sensor is used as the primary sensor for measuring the inventory of the condensate tank while a time domain reflectometer provides a supplementary level measurement.

The melt temperature is measured with a multi-junction probe made up of 4 C-type (W-5%Re/W-26%Re) thermocouples (Figure 2-8). The probe is mounted on the bottom flange of the RV and protected from the melt by a tungsten thermowell. The thermowell has a 6 mm o.d. and 1 mm wall, and the top end is positioned 100 mm above the bottom of the melt. The thermocouples are located 90, 65, 40, and 15 mm above the bottom of the melt.

Six C-type thermocouples are used to measure temperatures at the corium/lining interface to show whether water seeps around the edges of the melt to provide unwanted lateral cooling. Two thermocouples are positioned 150 mm above the base of the melt, two at 100 mm, and two at 50 mm. Instruments are listed in Table 2-1.

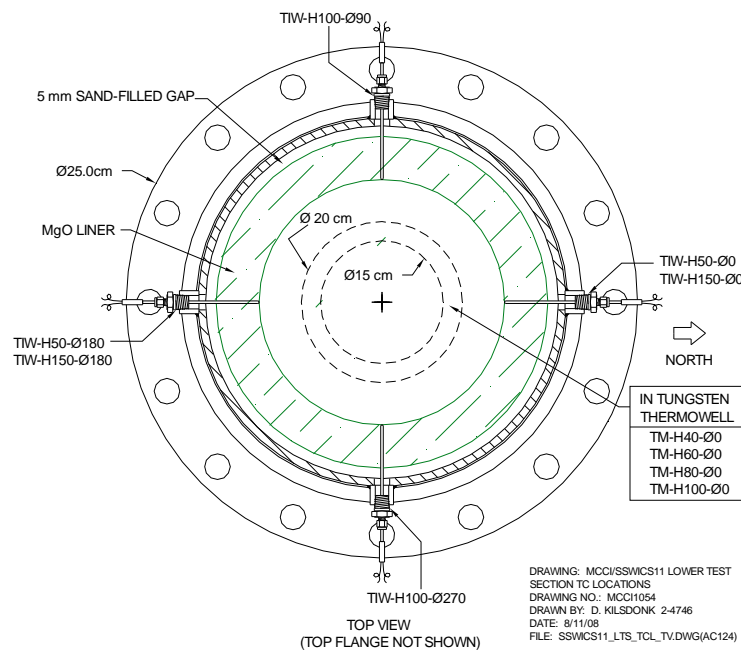


Figure 2-8. Instrumentation Positions in Basemat and Lower MgO Liner.

Table 2-1. Instrument List.

#	Channel	Name	Type	Description	Serial #	Output	Range	Accuracy
0	HPS-0	T-CJ-HPS	AD592 IC	Cold junction compensation sensor.	-	1µA/K	0-70°C	±0.5°C
1	HPS-1	TM-H100-Φ0	TC type C	Melt temp. 100 mm above bottom of melt (in tungsten thermowell).	-	0-37 mV	0-2320°C	±4.5°C or 1%
2	HPS-2	TM-H80-Φ0	TC type C	Melt temp. 80 mm above bottom of melt (in tungsten thermowell).	-	0-37 mV	0-2320°C	±4.5°C or 1%
3	HPS-3	TM-H60-Φ0	TC type C	Melt temp. 60 mm above bottom of melt (in tungsten thermowell).	-	0-37 mV	0-2320°C	±4.5°C or 1%
4	HPS-4	TM-H40-Φ0	TC type C	Melt temp. 40 mm above bottom of melt (in tungsten thermowell).	-	0-37 mV	0-2320°C	±4.5°C or 1%
8	HPS-8	TIW-H50-Φ0	TC type C	Melt temp. at inner sidewall 50 mm above bottom of melt.	-	0-37 mV	0-2320°C	±4.5°C or 1%
9	HPS-9	TIW-H50-Φ180	TC type C	Melt temp. at inner sidewall 50 mm above bottom of melt.	-	0-37 mV	0-2320°C	±4.5°C or 1%
10	HPS-10	TIW-H100-Φ90	TC type C	Melt temp. at inner sidewall 100 mm above bottom of melt.	-	0-37 mV	0-2320°C	±4.5°C or 1%
11	HPS-11	TIW-H100-Φ270	TC type C	Melt temp. at inner sidewall 100 mm above bottom of melt.	-	0-37 mV	0-2320°C	±4.5°C or 1%
12	HPS-12	TIW-H150-Φ0	TC type C	Melt temp. at inner sidewall 150 mm above bottom of melt.	-	0-37 mV	0-2320°C	±4.5°C or 1%
13	HPS-13	TIW-H150-Φ180	TC type C	Melt temp. at inner sidewall 150 mm above bottom of melt.	-	0-37 mV	0-2320°C	±4.5°C or 1%
18	HPS-18	TG-RV	TC type C	Gas temp. in reaction vessel upper plenum.	-	0-37 mV	0-2320°C	±4.5°C or 1%
22	HPS-22	TS-RV-tf	TC type K	Temperature of RV top flange.	-	0-50 mV	0-1250°C	±2.2°C or 0.75%
23	HPS-23	TS-RV-1000	TC type K	Outer wall temp. of RV 1000 mm above bottom of melt.	-	0-50 mV	0-1250°C	±2.2°C or 0.75%
24	HPS-24	TS-RV-mf	TC type K	Temperature of RV middle flange.	-	0-50 mV	0-1250°C	±2.2°C or 0.75%
25	HPS-25	TS-RV-100	TC type K	Outer wall temp. of RV 100 mm above bottom of melt.	-	0-50 mV	0-1250°C	±2.2°C or 0.75%
26	HPS-26	TS-RV-bf	TC type K	Temperature of RV bottom flange.	-	0-50 mV	0-1250°C	±2.2°C or 0.75%
27	HPS-27	TS-vent	TC type E	Outer wall temp. of vent line.	-	0-70 mV	0-900°C	±1.7°C or 0.5%
28	HPS-28	TF-CT-102	TC type K	Fluid temp. in condensate tank at a water level of 102 mm.	-	0-50 mV	0-1250°C	±2.2°C or 0.75%
29	HPS-29	TF-CT-406	TC type K	Fluid temp. in condensate tank at a water level of 406 mm.	-	0-50 mV	0-1250°C	±2.2°C or 0.75%
30	HPS-30	TF-CT-711	TC type K	Fluid temp. in condensate tank at a water level of 711 mm.	-	0-50 mV	0-1250°C	±2.2°C or 0.75%
31	HPS-31	TF-CT-1016	TC type K	Fluid temp. in condensate tank at a water level of 1016 mm.	-	0-50 mV	0-1250°C	±2.2°C or 0.75%
32	HPS-32	TF-CT-1321	TC type K	Fluid temp. in condensate tank at a water level of 1321 mm.	-	0-50 mV	0-1250°C	±2.2°C or 0.75%
33	HPS-33	TF-CT-1626	TC type K	Fluid temp. in condensate tank at a water level of 1626 mm.	-	0-50 mV	0-1250°C	±2.2°C or 0.75%
34	HPS-34	TF-HX-in	TC type K	Fluid temp. at HX coolant inlet.	-	0-50 mV	0-1250°C	±2.2°C or 0.75%
35	HPS-35	TF-HX-out	TC type K	Fluid temp. at HX coolant outlet.	-	0-50 mV	0-1250°C	±2.2°C or 0.75%
36	HPS-36	HF-vent	Thermopile	Heat Flux through connecting line to V-ST.	0632	0-5.50 mV	0-5 kW/m ²	±3%
38	HPS-38	TF-quench	TC type K	Temperature of water injected into RV	-	0-50 mV	0-1250°C	±2.2°C or 0.75%
40	HPS-40	PA-RV	1810AZ	Absolute pressure in reaction vessel.	02351-00P1PM	1-6 V	0-14 bar gage	±0.14 bar
41	HPS-41	PD-CT	1801DZ	ΔP transmitter to measure condensate inventory.	D-9	0-13 V	0-0.35 bar	±0.004 bar
42	HPS-42	L-TDR-CT	BM100A	Time domain reflectometer to measure CT level.	A02331879A	4 - 20 mA	0 - 2 m	±3 mm
44	HPS-44	F-sparg	HFC-203	Flow rate of argon into injector for gas sparging	3621300001	0 - 5 V	0-50 sl/m Ar	±0.5 sl/m
60	HPQ-50	T-CJ-HPQ	AD592 IC	Cold junction compensation sensor.	-	1µA/K	0-70°C	±0.5°C
61	HPQ-51	TF-ST	TC type K	Fluid temp. in spray tank.	-	0-50 mV	0-1250°C	±2.2°C or 0.75%
62	HPQ-52	TG-CL-out	TC type K	Gas temperature in condensate tank outlet line to spray tank.	-	0-50 mV	0-1250°C	±2.2°C or 0.75%
63	HPQ-53	TG-ST-in	TC type K	Gas temp. in the spray tank line inlet.	-	0-50 mV	0-1250°C	±2.2°C or 0.75%
64	HPQ-54	TG-ST-out	TC type K	Gas temp. in the spray tank line outlet.	-	0-50 mV	0-1250°C	±2.2°C or 0.75%
65	HPQ-55	F-quench	Paddlewheel	Flow rate of water into reaction vessel (for quenching melt).	3144	0-5 V	0-50 gpm	±0.5 gpm
66	HPQ-56	F-HX	Paddlewheel	Flow rate of cold water to heat exchangers.	3143	0-5 V	0-50 gpm	±0.5 gpm

2.5 Results

The revised injector configuration with tungsten capillaries extending up into the melt succeeded in preventing the gas bypass that was observed in SSWICS-8. Post test examinations revealed an ingot morphology that differed from any of the other tests. The ingot did not bond to the MgO liner as usual, but instead bonded strongly to the basemat. This permitted removal of the liner by simply lifting it up from the basemat so that the perimeter of the ingot could be examined. The ingot is shown in Figure 2-9. The smooth white-green material around the outer surface is the remains of the zirconia felt used to cover the inside of the liner. The felt is normally white and most of it was scraped away to reveal the corium below.

The ingot proved to be a solid mass without the coarse crack network present in earlier specimens. It also had an unusually porous appearance that can be seen upon close examination of Figure 2-10. The extensive array of dimples/holes is unique among the SSWICS ingots. The ingot mass is ~61.8 kg, which is calculated by subtracting the 6.2 kg of corium attached to the liner walls above the ingot from the initial thermite mass of 68 kg. The porosity is estimated to be roughly 37%, which is calculated from the ingot mass, a density of 6000 kg/m³, and an approximate average height of 23 cm. Note that the heights of both the SSWICS-6 and -8 ingots were about 15 cm though they had the same composition and mass. Figures 2-11 and 2-12 are provided for further consideration of the differing ingot morphologies. The surface of Ingot 6 is uneven but rather smooth except for the orange region which is chromium left over from the chemical reaction used to create the melt. In addition, there are no readily evident cracks. Ingot 11, on the other hand, has a very rough surface with a significant gap at the perimeter. Sparging clearly plays a role in adding melt porosity beyond what is normally generated by thermal stress cracking.

The melt cooling rate was measured for comparison with previous tests. Melt temperatures measured by the multi-junction thermocouple in the tungsten thermowell are shown in Figure 2-13. The melt cooled from its peak temperature of ~1850°C to 100°C in 1 ½ hours, which is faster than all other tests except SSWICS-7, which had the least amount of concrete at 4%. Figure 2-14 shows the calculated heat flux derived from measurements of condensed steam flow and from an energy balance on the heat exchanger that condenses the steam. Two independent measurements are used within the condensate tank: a differential pressure sensor (DP) that measures water column head and a time domain reflectometer that measures water column height. The heat exchanger energy balance is derived from a flow measurement on the HX secondary side along with inlet and outlet thermocouples. Details of the data reduction can be found in the data report [4].

Figure 2-15 compares the cooling rates during SSWICS-6, -8, and -11. As noted earlier, the injected argon circumvented the melt in SSWICS-8 and so it was effectively a repeat of SSWICS-6. The plot shows that the cooling rates correspond well for the two tests. In the next section it will be shown that there is also similarity in the structural strength of the SSWICS-6 and -8 crusts. Though this repetition of SSWICS-6 was accidental, it is useful in supporting the notion that these tests are repeatable.

Figure 2-16 shows the cooling rates for all of the ~70-80 kg quench tests (SSWICS-9 and -10 were 25 kg and are discussed in the next section). It can be seen that SSWICS-11, with its comparatively high concrete content, cooled at a rate more comparable to the low concrete melts. Only SSWICS-7, with the lowest tested concrete content, quenched more quickly. Note also that melts with high cooling rates seem to plateau early in the transient, which we have associated with a dryout limit. SSWICS-11 does not exhibit a plateau, which may be because this relatively small melt, which lacks internal heating, is unable to sustain extremely high heat fluxes long enough to produce a plateau.



Figure 2-9. Corium Side View of Ingot 11.

Figure 2-10. Corium at Level of Top of Tungsten Thermowell after Removal of Upper Layers (Ingot 11).





Figure 2-11. Top View of Ingot-6 Ingot Within Liner.

Figure 2-12. Top View of Ingot-11 Ingot before Liner Removal.



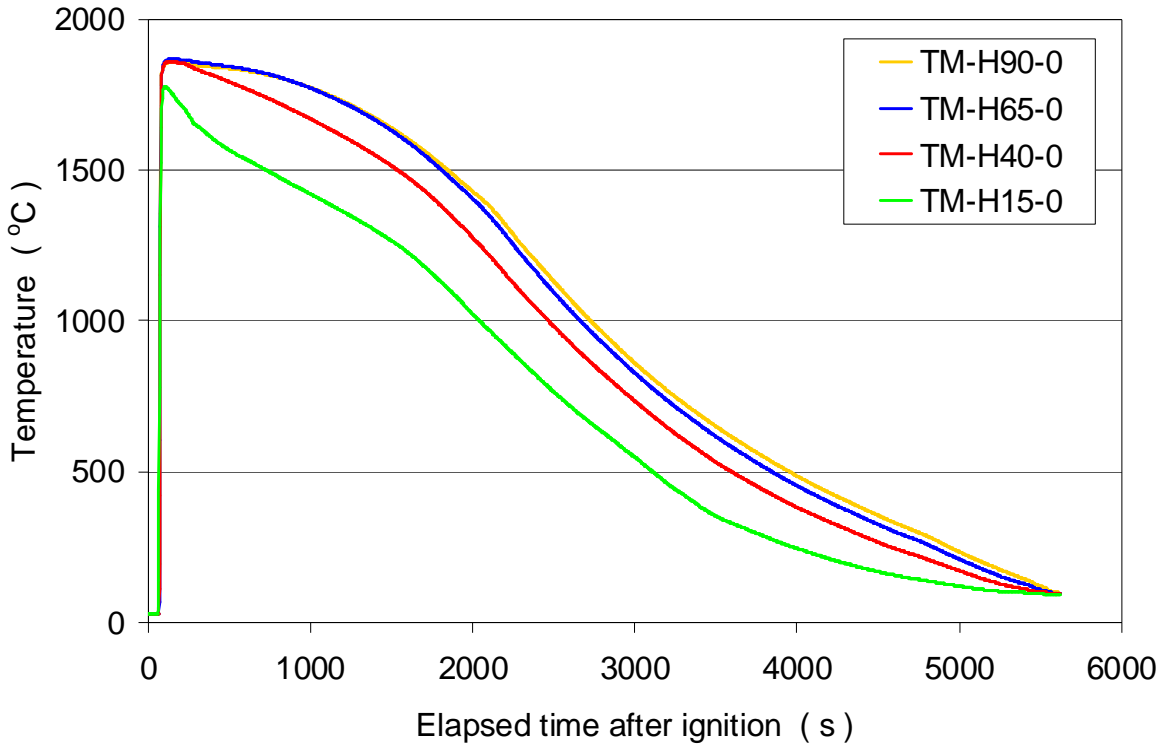
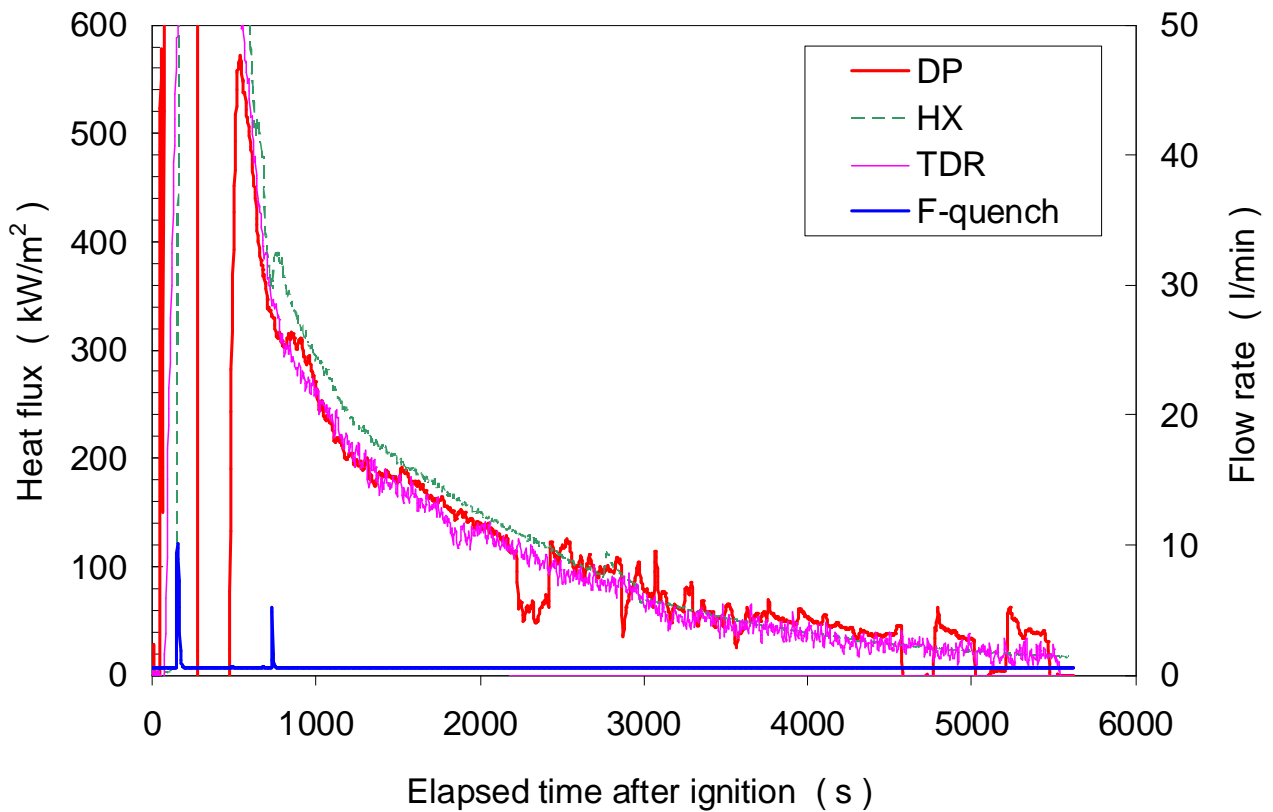


Figure 2-13. SSWICS-11 Temperatures in Tungsten Thermowell.

Figure 2-14. SSWICS-11 Calculated Corium Surface Heat Flux.



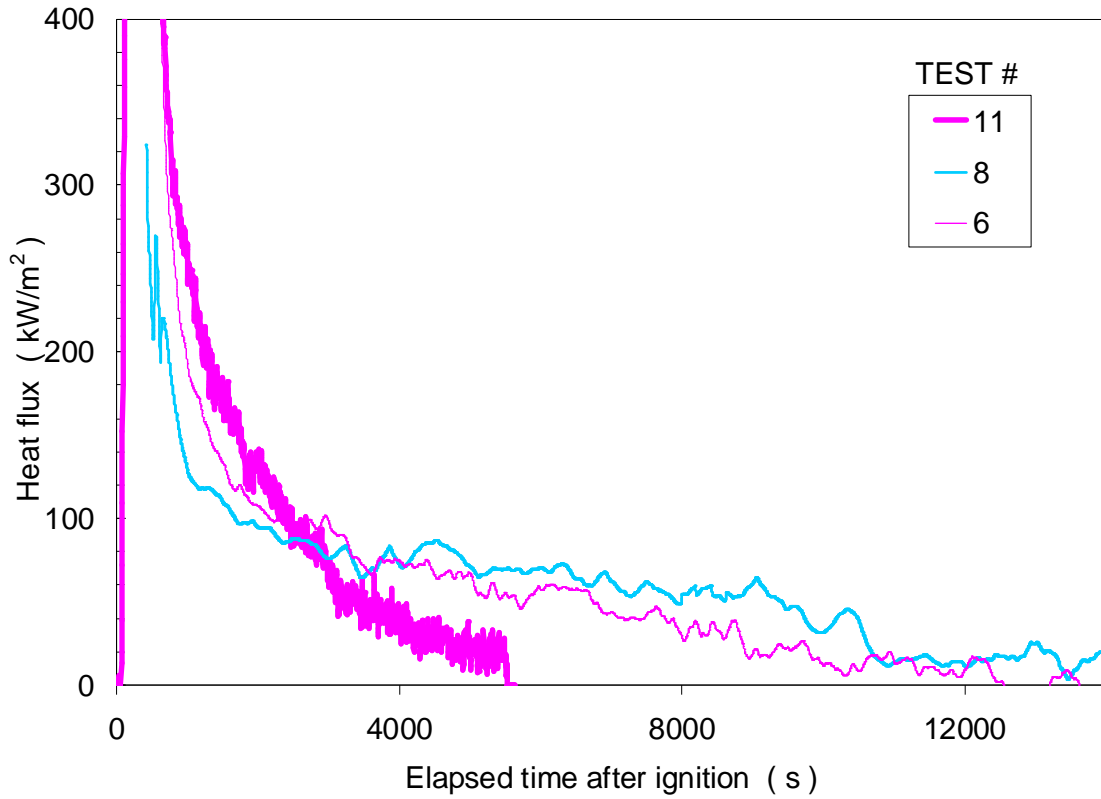
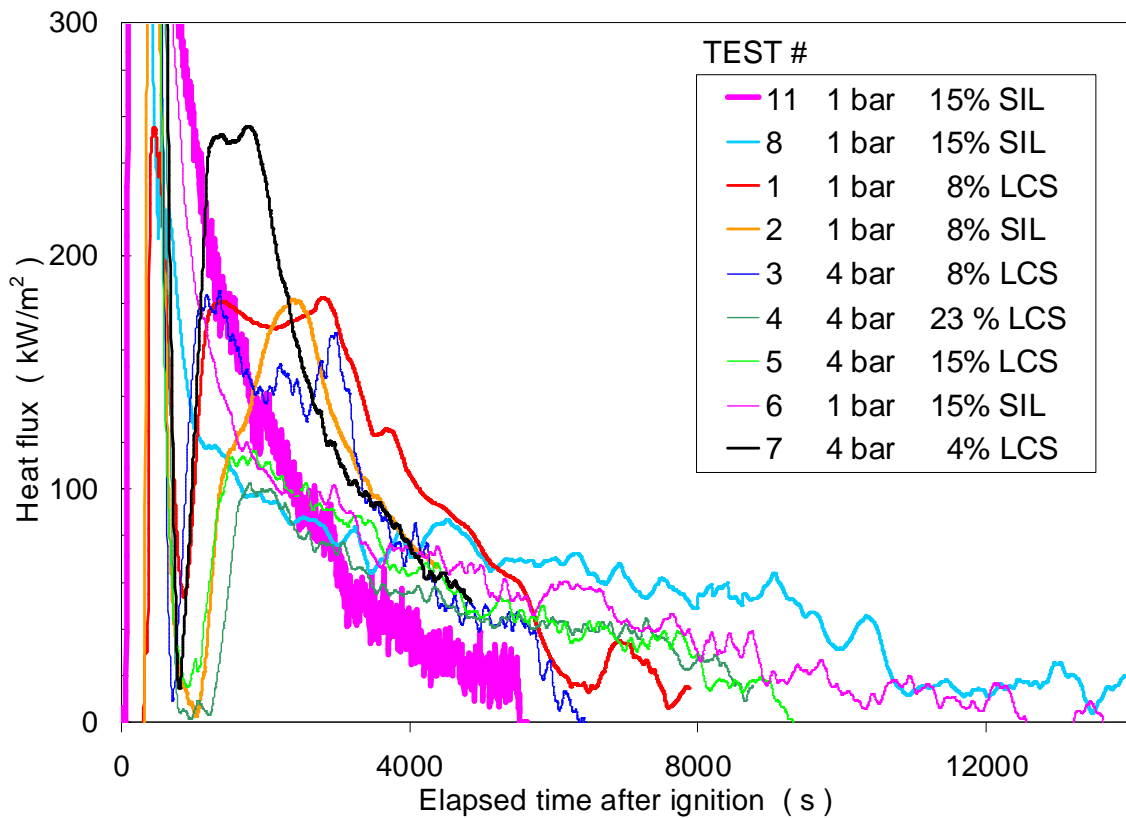


Figure 2-15. Heat Flux for Tests with Sparging (11) and Without (8 & 6). The Melt Composition and Quench Conditions are Identical for the Three Tests.

Figure 2-16. Calculated Heat Flux for all Nine Quench Tests.



3.0 CRUST STRENGTH TESTS

Along with the quench rate measurements, the SSWICS separate effects experiments included measurements of corium crust strength. The purpose of collecting such data is to aid in the assessment of the potential stability of an anchored corium crust within a power plant. A crust that anchors to the containment walls could hinder heat transfer from an overlying water layer down to the melt below. A crust with few flaws is thought to be more stable than one permeated with cracks. Measurements of the structural strength of corium can be useful in gauging the strength of a plant-scale crust, but specimens must be large enough to contain a representative sampling of the cracks and voids one would expect in an actual corium crust. The quench tests described in the preceding section produced ingots that met this requirement.

The quench tests were designed to optimize measurements of heat flux from the corium surface and consequently the ingots were not of optimal thickness for the strength measurements. A minimum corium depth of 150 mm was considered necessary to obtain a satisfactory heat flux measurement. However, 150 mm is too large for optimal load testing and so the ingots were sectioned (cut in the radial direction) to increase their aspect ratio (diameter/thickness) to make them more suitable for load testing. Unfortunately, the cutting process is laborious and involves much handling of the ingot, increasing uncertainty that mechanical strength is not significantly changed before the load test. This uncertainty would be eliminated if the ingots produced by the quench tests could be tested without having to cut them.

SSWICS-9 & 10, in contrast to previous tests, were designed to optimize the ingot thickness for load testing. A reduced amount of corium was used in the quench test to produce a thinner ingot. The ingot was then load tested without sectioning. The following sections summarize the test conditions and results of these two tests and compare them to strength measurements performed in the previous program.

3.1 Test Results

The reaction vessel and auxiliary systems are essentially the same as those described in Section 2.3, though somewhat simplified as no sparging system was used. A side view of the reaction vessel is shown in Figure 3-1. Melt mass for these two tests was 25 kg instead of the usual ~70 kg to produce a 50 mm high ingot. Usually melt temperature is measured with a thermocouple within a tungsten thermowell projecting up from the basemat into the melt, but it was omitted to avoid creating a potential weak spot in the specimen. Corium compositions and test conditions for SSWICS-9 and -10 match those of SSWICS-6 and -2, respectively. A complete table of the SSWICS quench tests is provided in Table 3-1.

The ingots for both SSWICS-9 and -10 were created by performing a quench test in the same fashion as that of the larger-melt tests. System conditions such as pressure and temperature were duplicated with water addition from above. The intention was to reproduce the thermal stress cracking mechanisms that produced the crack structure within the thicker ingots. The cooling rate of these smaller ingots is of little interest since lateral heat losses are relatively large and the corium cools too quickly to allow a determination of the dryout heat flux. Therefore temperature traces and heat flux plots are not included here. They are, however, available in the data reports [5, 6].

The ingot produced by the SSWICS-9 quench test was the first one that failed to bond to the MgO liner, which effectively supports the corium when transported and placed on the loading apparatus and, for the thicker ingots, during the cutting process. Because of this lack of bonding Ingot 9 broke apart

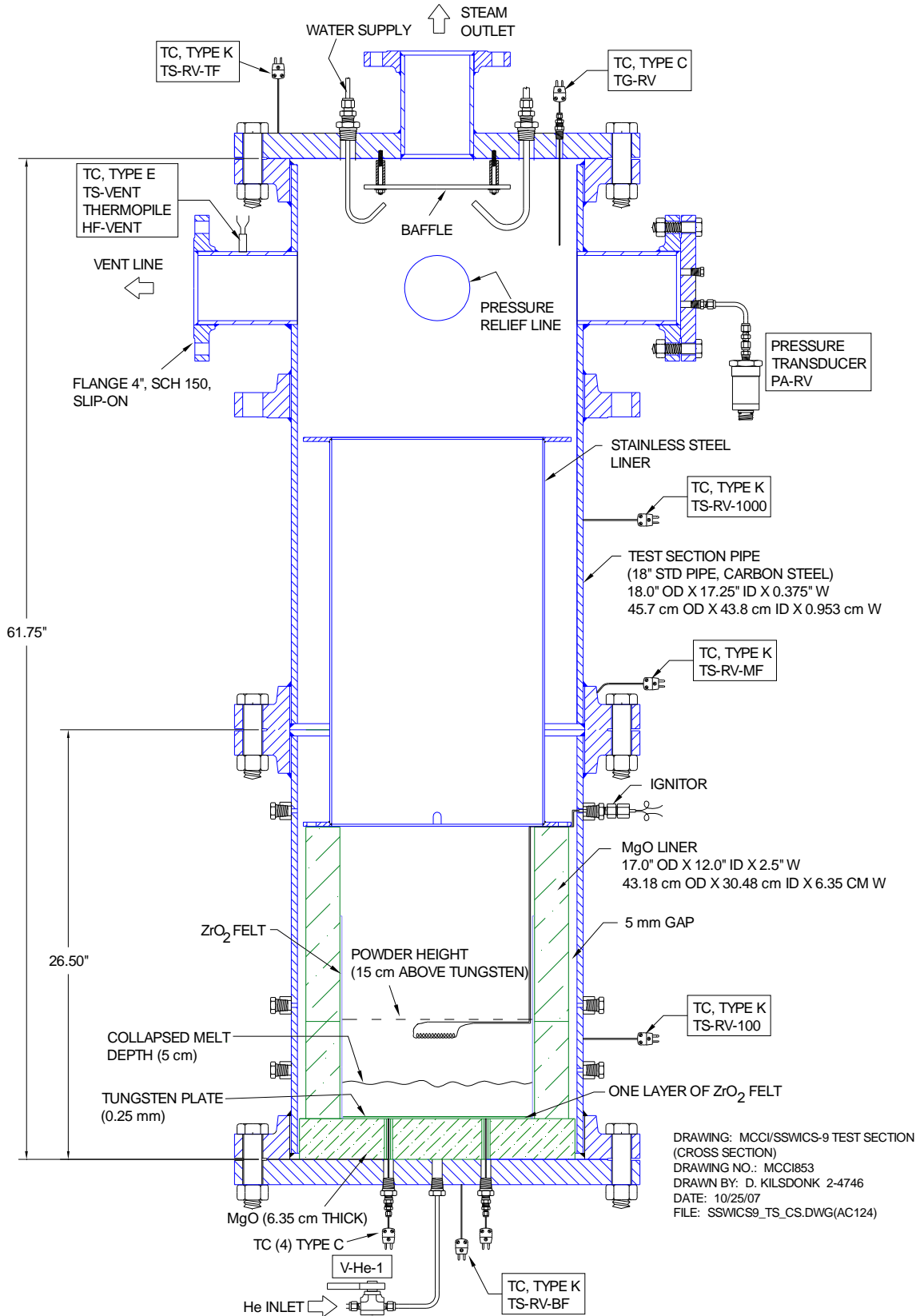


Figure 3-1. Side View of Reaction Vessel for SSWICS-9 and -10.

Table 3-1. Test Specifications for SSWICS Quench Experiments.

Parameter	Test Number										
	1	2	3	4	5	6	7	8	9	10	11
Melt composition (wt% UO ₂ /ZrO ₂ /Cr/Concrete)	61/25/6/8	61/25/6/8	61/25/6/8	48/20/9/23	56/23/7/14	56/23/6/14	64/26/6/4	56/23/6/14	56/23/6/14	61/25/6/8	56/23/6/14
Concrete type	LCS	SIL	LCS	LCS	LCS	SIL	LCS	SIL	SIL	SIL	SIL
Melt mass (kg)	75	75	75	60	68	68	80	68	23	25	68
Melt depth (cm)	15	15	15	15	15	15	15	15	5	5	15
Initial Melt Temperature (°C)	~2300	~2100	~2100	~2100	~2100	~1950	~2100	~1900	-	-	~1850
System pressure (bar)	1	1	4	4	4	1	4	1	1	1	1
Water injection flowrate (lpm)	4	4	12	13	6	14	13	10	9	9	-
Water injected (liters)	33	39	34	40	61	47	40	41	20	29	>30
Test date (day/mo/year)	30/08/02	17/09/02	30/01/03	13/03/03	15/10/03	24/02/04	14/12/04	25/01/07	14/02/08	5/03/08	11/05/08

during removal from the basemat and was unsuitable for load testing. Ingot 10, however, was successfully moved and tested.

The load test apparatus and calculation of sample strength have been described in an earlier report [7] and will not be described in detail here. The apparatus uses a piston to apply a point load to the center of the ingot. Sensors attached to the upper and lower surfaces of the sample measure displacement during loading. Figure 3-2 shows the sample stress, calculated from the applied load, versus time. Included in the plot are measured displacements of the upper and lower surfaces. The two measurements move in tandem and this is an indication that the sample is, roughly speaking, bending rather than being crushed.

The peak load at failure was 1.4 kN with the resultant calculated strength equal to 1 MPa \pm 0.3 MPa. The uncertainty value is derived from variance in the sample thickness (\pm 5 mm), which is believed to be the largest source of uncertainty in the calculation of strength from the peak load.

Figure 3-3 is a plot of ingot strength for all of the tested ingots. It can be seen that the strength of sample is very close to that of Ingot-2, which had the same chemical composition. Details of each sample are provided in Table 3-2 for reference.

Figure 3-3 also includes crust strength measurements made during two CCI (core-concrete interaction) tests. These are in-situ measurements made during the melt quench process and are an indication of the strength of a high temperature crust with a large temperature gradient. The top surface of the crust was held near 100°C by the overlying layer of boiling water while the underside was \sim 2000°C. The CCI crusts proved to be weaker than the room temperature SSWICS samples, suggesting that the SSWICS measurements provide a conservative estimate of corium crust strength. Additional discussion of the implications of the measurements of corium crust strength can be found in [8].

Table 3-2. Source Data for Calculation of Section Strength.

Ingot number	1	2	3	4		5		6			8	10
Slab thickness (mm)	100	100	90	55-60	55-60	55	45	50	55	40	50	50
Aspect ratio	3	3	3.3	5	5	5.4	6.7	6	5.4	7.5	6	6
Region of ingot*	T	T	T	M	B	M	B	T	M	B	M	-
Concrete content (%)	8	8	8	23	23	14	14	14	14	14	14	8
Peak load (kN)	8.2	8.2	15.3	3.2	2.7	3.6	4.4	4.5	4.1	3.0	2.4	1.4
σ_{max}	1.1	1.1	2.7	1.6	1.3	2.0	3.6	3.0	2.2	3.2	1.6	1.0
Stress uncertainty (MPa)	0.2	0.2	0.4	0.3	0.3	1.0	0.8	1.0	0.5	0.7	0.4	0.3
Top surface Δz at peak load (mm)	10.0	9.1	8.2	2.4	5.3	2.3	2.4	5.0	3.8	4.8	-	5.9
Bottom surface Δz at peak load (mm)	-	-	-	-	-	2.1	2.2	8.9	3.2	3.8	-	3.9

* T = top; M = middle; B = bottom segment.

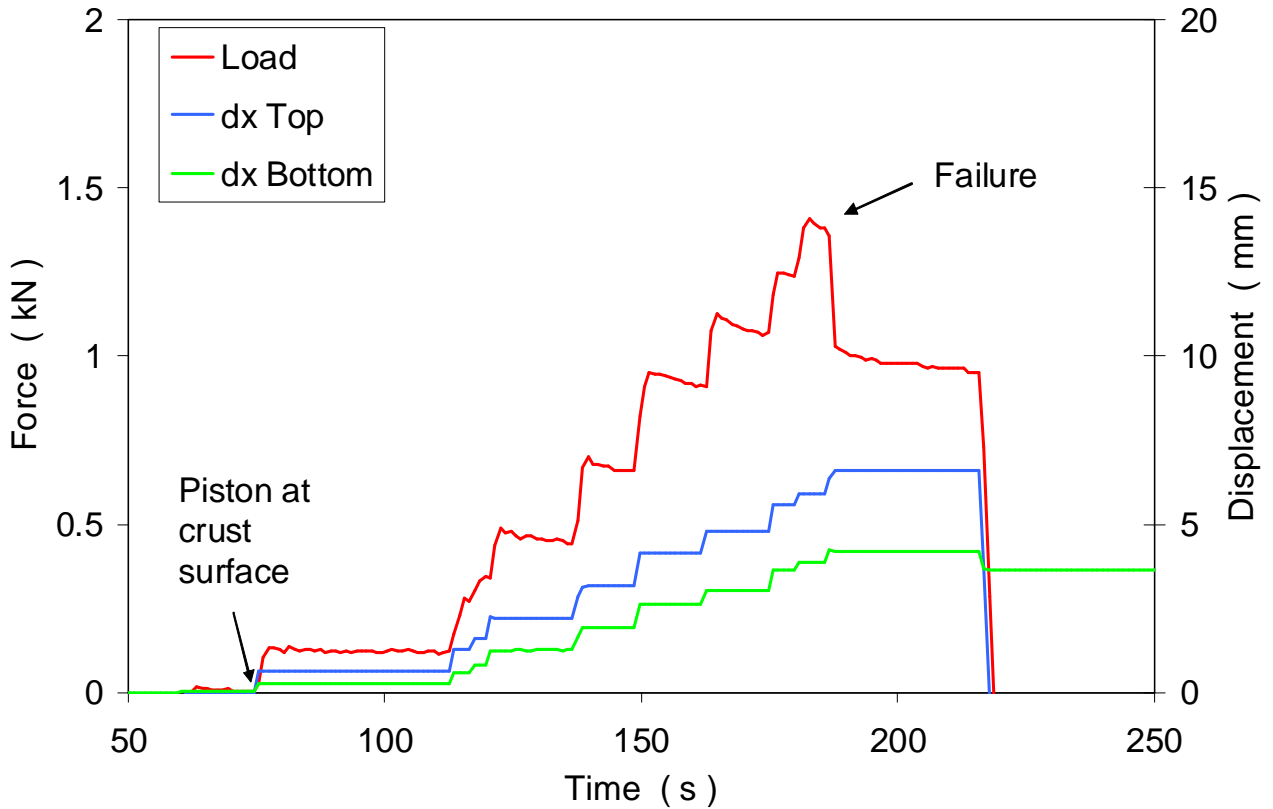
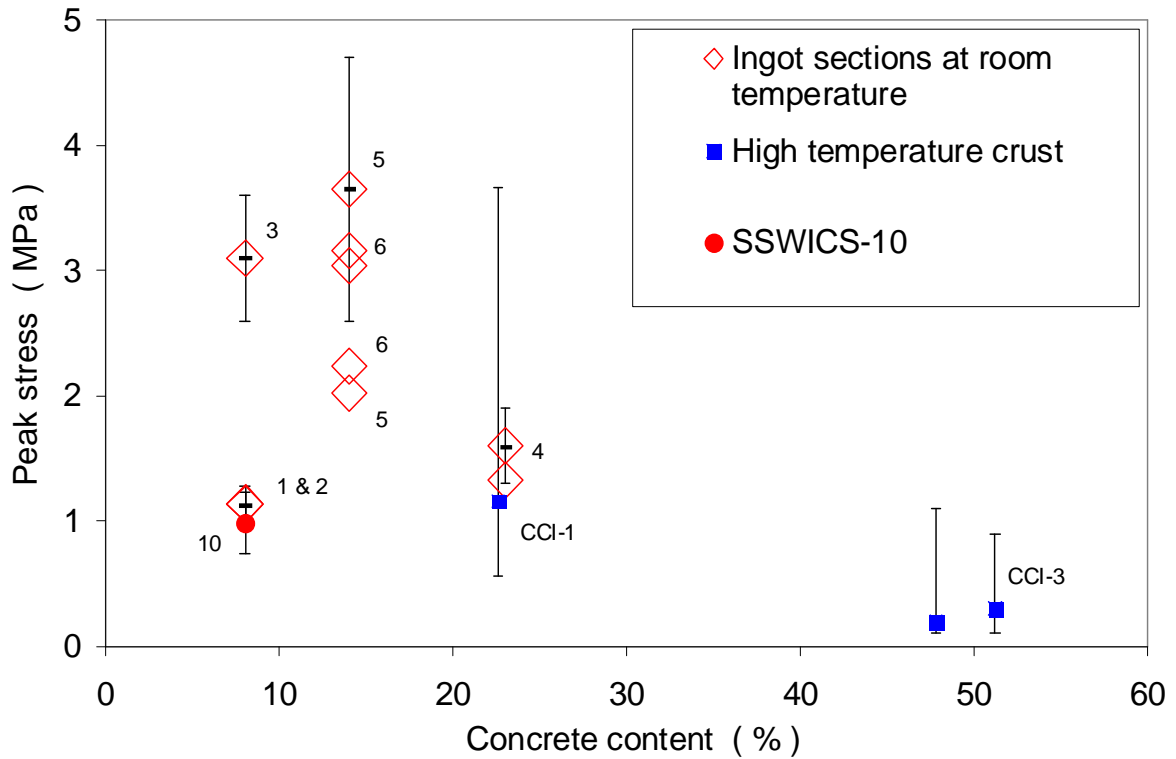


Figure 3-2. Ingot 10 Load Test.

Figure 3-3. Measured Strength of SSWICS Room Temperature Samples and In-Situ Measurements of Crust Strength in CCI-1 and CCI-3.



4.0 REFERENCES

1. M. T. Farmer, D. J. Kilsdonk, and R. W. Aeschlimann, "MSET-1 Test Data Report," EPRI/MACE-TR-D18, January, 2002.
2. S. Lomperski, M. T. Farmer, D. J. Kilsdonk, and R. W. Aeschlimann, "Small-Scale Water Ingression and Crust Strength Tests (SSWICS); SSWICS-8 Test Data Report: Thermalhydraulic Results," OECD/MCCI-2007-TR02, April 2007.
3. S. Lomperski, M. T. Farmer, D. J. Kilsdonk, and R. W. Aeschlimann, "Small-Scale Water Ingression and Crust Strength Tests (SSWICS); SSWICS-11 Design Report," OECD/MCCI-2008-TR05, August 2008.
4. S. Lomperski, M. T. Farmer, D. J. Kilsdonk, and R. W. Aeschlimann, "Small-Scale Water Ingression and Crust Strength Tests (SSWICS); SSWICS-11 Test Data Report: Thermalhydraulic Results," OECD/MCCI-2009-TR01, September 2009.
5. S. Lomperski, M. T. Farmer, D. J. Kilsdonk, and R. W. Aeschlimann, "Small-Scale Water Ingression and Crust Strength Tests (SSWICS); SSWICS-9 Test Data Report: Thermalhydraulic Results," OECD/MCCI-2008-TR01, February 2008.
6. S. Lomperski, M. T. Farmer, D. J. Kilsdonk, and R. W. Aeschlimann, "Small-Scale Water Ingression and Crust Strength Tests (SSWICS); SSWICS-10 Test Data Report: Thermalhydraulic Results," OECD/MCCI-2008-TR02, March 2008.
7. S. Lomperski, M. T. Farmer, D. J. Kilsdonk, R. W. Aeschlimann, and S. Basu, "Small-Scale Water Ingression and Crust Strength Tests (SSWICS); SSWICS Final Data Report: Crust Strength Measurements," OECD/MCCI-2005-TR02, June 2005.
8. S. Lomperski and M. T. Farmer, "Corium Crust Strength Measurements," Nuclear Engineering and Design, Vol. 239, pp. 2551-61, 2009.